A Closed-Form Multiscale Thermal Contact Resistance Model

Robert L. Jackson, Hamed Ghaednia, Yasser A. Elkady, Sushil H. Bhavnani, and Roy W. Knight

***Abstract*— All surfaces are rough to some extent and therefore only a small portion of surfaces actually comes into contact when they are brought together. Therefore heat flow from one object to another is retarded by this incomplete contact, resulting in thermal contact resistance (TCR). Minimizing the TCR is important for many different applications where dissipating heat is important, such as in micro- and high-power electronics. This paper presents a simplified closed-form method for modeling TCR while considering the multiscale nature of surfaces in the contact mechanics and heat transfer theory. When modeling the contact between surfaces, it is important to consider the multiple scales of roughness that exist. Many rough surface contact models exist in the recent literature, but they can be difficult to implement and use for TCR predictions. This paper derives and presents a simplified closed-form multiscale model of TCR. The results are then compared with experimental measurements of the TCR for copper samples and with other existing models. The comparison shows relatively close agreement with the closed-form multiscale model.**

***Index Terms*— Contact mechanics, elastic–plastic, roughness, scale-dependent properties, surface contact.**

NOMENCLATURE

A_i	Area of contact for a particular scale.
A_n	Nominal contact area.
A_r	Real contact area.
A_s	Cross-sectional area of test sample.
a, b, c	Empirical correlation coefficients.
a_c	Radius of the single asperity area of contact.
B	Ratio of asperity amplitude Δ to wavelength λ.
c_o	Empirical quantity.
d	Separation of mean asperity height.
E	Elastic modulus.
E'	Equivalent elastic modulus: $\left((1-\upsilon_1^2)/E_1 + (1-\upsilon_2^2)/E_2\right)^{-1}$.
F	Contact force.
f	Spatial frequency (reciprocal of wavelength).
H	Hardness of the softer surface ($H \approx 2.84 S_y$).
H_m	Microhardness of the softer surface.
h^*	Material-dependant length scale.
h_p	Depth of plastic deformation.
h_c	Thermal contact conductance ($1/R_c$).
K	Harmonic mean thermal conductivity of surface materials.
k_s	Thermal conductivity of sample material.
L_s	Sample thickness.
M_2	Second moment of the surface.
M_4	Fourth moment of the surface.
m	Effective absolute surface slope.
N	Total number of surface data points.
n	Number of contact spots (asperities in contact).
P	Nominal contact pressure, F/A_n.
P_r	Real contact pressure, F/A_r.
P^*	Average pressure for complete contact.
Q	Heat flowing through the test system.
Q_{10}	Measured heat flow through 10-mm sample.
Q_5	Measured heat flow through a 5-mm sample.
R_c	Thermal contact resistance.
$R_{\text{th\_10 mm}}$	Thermal resistance of a 10-mm sample.
$R_{\text{th\_5 mm}}$	Thermal resistance of a 5-mm sample.
S_y	Yield strength.
ΔT_s	Temperature drop across sample.
ΔT_{10}	Measured temperature drop across a 10-mm sample.
ΔT_5	Measured temperature drop across a 5-mm sample.
x	Lateral asperity position.
z	Height of asperity measured from the mean of asperity heights.

GREEK SYMBOLS

α	Thermal expansion coefficient.
β	Average asperity radius of curvature.
η	Areal density of asperities.
σ	Effective standard deviation of surface heights (root mean squared roughness).
λ	Asperity wavelength.
Δ	Asperity amplitude.
Φ	Distribution function of asperity heights.
ω	Interference between hemisphere and surface.
ν	Poisson's ratio.

Manuscript received October 21, 2011; revised February 14, 2012; accepted March 27, 2012. Date of publication May 15, 2012; date of current version June 28, 2012. Recommended for publication by Associate Editor P. Dutta upon evaluation of reviewers' comments.

R. L. Jackson, H. Ghaednia, S. H. Bhavnani, and R. W. Knight are with the Department of Mechanical Engineering, Auburn University, Auburn, AL 36849-5341 USA (e-mail: robert.jackson@eng.auburn.edu; hzg0004@tigermail.auburn.edu; bhavnsh@auburn.edu; knighrw@auburn.edu).

Y. A. Elkady is with the Engineering Faculty, Ras Al Khaimah College, Higher Colleges of Technology, Abu Dhabi 25026, UAE (e-mail: yakady@hotmail.com).

Color versions of one or more of the figures in this paper are available online at http://ieeexplore.ieee.org.

Digital Object Identifier 10.1109/TCPMT.2012.2193584

SUBSCRIPTS

asp	Single asperity.
c	Critical value at onset of plastic deformation.
def	Deformed value.
i	Frequency level or scale.
max	Maximum value.
o	Bulk property.
p	Elastic-plastic.
t	Adjusted for thermal expansion.

I. INTRODUCTION

ECONOMICALLY improving the heat conduction from high-power systems, microelectromechanical systems, and microelectronics is a growing issue in the industry because the size of electronic devices continues to decrease. The decrease in the size of electronic devices reduces the available surface area for heat dissipation, leading to large increases in heat flux. This can lead to increases in operating temperatures that exceed the design criteria. Thus, the thermal contact resistance (TCR) between these devices and a heat sink is very important, as it limits the rate at which heat can be dissipated. It is well known that the roughness between contacting surfaces can reduce the real area of contact and thus restricts the heat flow, which is seen as an increase in the TCR (see Fig. 1).

Although there has been a large amount of work investigating TCR [1]–[4], there are some severe problems with the current methods used to predict it. Lambert and Fletcher [1] summarized the currently used theoretical and empirical TCR models as "these do not agree with most results for an arbitrarily nonflat, rough surface, those usually obtained from common manufacturing processes. Empirical and semiempirical correlations, although many are developed for nonflat, rough surfaces, also suffer from limited applicability."

In addition, these dated theoretical models make use of contact mechanics techniques which have since been proven to have significant pitfalls. For instance, the very popular Greenwood and Williamson (GW) [5] statistical model has been shown to produce results that are dependent on the resolution of the surface profiling device [6]–[8], but may still be useful and applicable in some situations. In addition, most other models that attempt to correct this issue by using fractal mathematics [9]–[16] assume that a surface can be characterized as self-affine, or follow a given structure for each scale of roughness, when in reality no real surface is truly self-affine.

Many existing models assume that the contact pressure equals the hardness at high loads, and that it is a constant at approximately three times the yield strength. Several researchers have shown that this hardness varies with scale, with the deformed geometry, and with other material properties [8], [17]–[26], and was thus incorrectly employed in the previous models. For these reasons, several researchers have recently developed new multiscale contact models [27]–[31] to alleviate these problems, although they are still being refined. The work by Li *et al*. [8] even examined the dependence of the statistical parameters necessary for the GW model to predict TCR and also the scale dependence of the microhardness. This paper refines the new multiscale theory for the TCR between rough surfaces and compares it with the existing model by Yovanovich and coworkers [4]. Several researchers have also explored using deterministic models of rough surface contact for predicting TCR, but these techniques can be very expensive computationally [32], [33].

More recently, Jackson *et al*. [34] demonstrated a multiscale model of TCR based on Archard's stacked asperity model. The model used Jackson and Streator's purely mechanical rough surface contact methodology which employed a Fourier transform to obtain quantitative descriptions of each stacked scale [27]. The model also considered the effect of scale-dependent thermal conductivity [35]–[41], and showed that the average size of the contact spots is usually large enough so that the scale dependence plays only a minor role. However, the scale-dependent yield strength [20], [23], [42]–[47] of the smaller asperities in contact does appear to have a significant effect and has not been thoroughly investigated with respect to TCR.

Although many of these models may be used, some also require extensive calculations and coding to implement. The objective of this paper is to simplify the multiscale model and use it to evaluate the effect of scale-dependent surface features and properties on TCR.

Following the popular semiempirical methodology of Song and Yovanovich [4], [48], a simplified dimensional correlation of the analytical solution for the contact conductance is represented as

$$h_c = \frac{1}{R_c} = 1.25\, k\, \frac{m}{\sigma} \left(\frac{P}{H_m}\right)^{0.95} \tag{1}$$

where

$$k = \frac{2\, k_1\, k_2}{k_1 + k_2} \tag{2}$$

is the harmonic mean thermal conductivity of the contacting surfaces, $m = [m_1^2 + m_2^2]^{1/2}$ is the effective absolute surface slope, $\sigma = [\sigma_1^2 + \sigma_2^2]^{1/2}$ is the effective root mean square (RMS) surface roughness in micrometers, R_c is the TCR, P is the contact pressure in N/m^2, and H_m is the microhardness of the softer material in N/m^2. It should be noted that it can be difficult to find a universally acceptable method to calculate m. Equation (1) is also based on the "truncation" model, which assumes that the contact area will equal the force divided by the microhardness H_m. H_m is also dependent on the deformed geometry and the scale of the contact, as discussed previously. The effective microhardness has been correlated to the bulk hardness for several metals [23], [49]. We are unaware of any material that has adequately been characterized using the microhardness theory and also theories on the scale-dependent properties that will be discussed and used in the current model. From [48], the resulting correlation is

$$\frac{P}{H_m} = \left[\frac{P}{H\left(1.62 \cdot 10^{12} \cdot \sigma/m\right)^{c_o}}\right]^{\frac{1}{1+0.071 c_o}} \tag{3}$$

where c_o is -0.26. These equations will be compared with those of the new model which considers multiscale effects. Although the model by Song and Yovanovich does not directly

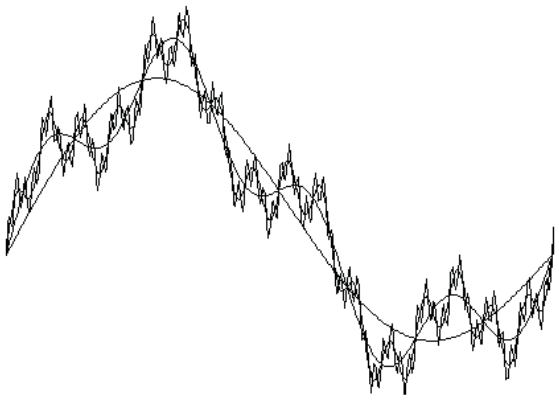

Fig. 1. Schematic depicting the decomposition of a surface into superimposed sine waves. Each line represents a different scale of roughness.

consider the effects of multiscale surface features or scale-dependent material properties, the use of the empirical microhardness theory appears to have been effective in including these scale effects.

The key to analytically predicting the TCR is to predict the real contact area and the distribution of the individual asperity contacts via a rough surface contact model. As mentioned, there are many different theoretical methods to model the contact of rough surfaces including deterministic [50], statistical [5], fractal [13], and multiscale models [27], [30], [34], [51]. Deterministic models if implemented with an adequate mesh density can provide effective predictions of TCR but can be computationally expensive. The methods based on fractal mathematics were derived to account for different scales of surface features not accounted for by the statistical models. The multiscale models were developed to alleviate the assumption of self-affinity imposed by fractal mathematics and also improve how the mechanics are considered. This paper employs a multiscale method that uses a Fourier transform to convert the surface profile data into a series of stacked sinusoids (see Fig. 1).

However, many of the above models require complex numerical methods in order to predict the real area of contact and then the TCR. There are only a few closed-form models that are available and widely used in the field, but they may also oversimplify the contact mechanics. To predict the real area of contact, probably the simplest method assumes that the real contact pressure is equal to Tabor's hardness [52]

$$A_r = \frac{F}{H} = \frac{F}{2.84 \cdot S_y}. \tag{4}$$

Pullen and Williamson later experimentally found that the real contact pressure was often higher than the predicted hardness [53], which was also found theoretically by the model used in this paper [24], [25]. This phenomenon was labeled "asperity persistence" and is due to the lateral interaction between asperities causing the stress state to become hydrostatic (see [25] and [54]).

This paper uses mostly the same underlying assumptions as the multiscale rough surface contact model by Jackson and Streator [27], except that the asperities are modeled as wavy or sinusoidal surfaces instead of spheres. The multiscale model derived by [27] uses the same direction of thought as Archard [55], but provides a method that can be easily applied to real surfaces. Jackson, Bhavnani, and Ferguson [34] used the concept to formulate a theoretical model of TCR which also included the effects of scale-dependent yield strength and thermal conductivity. It was found that the scale dependence of thermal conductivity may actually be negligible in TCR, but that scale-dependent yield strength may play a significant role, as was also found in [4], [23], [47], [48], and [56]. Both [27] and [34] used spherical contact models to consider individual elastic-plastic asperity contact. Wilson *et al*. [57] updated the multiscale model by using a more accurate elastic-plastic model of sinusoidal contact [24], [25], and also formulated a methodology to predict surface separation. The model presented by Wilson *et al*. [57] does not consider scale-dependent material properties, nor does it present a simplified closed-form solution as is done in this paper, but it is very similar to the "full multiscale model" without scale effects that is compared in the current simplified model and other results later in this paper. For a more in-depth description of the multiscale model, refer [27], [57], and [58].

II. Model Methodology

A. Simplified Multiscale Contact Model

The contact mechanics framework used in the multiscale model were derived by Jackson and Streator [27]. First, a fast Fourier transform (FFT) is performed on the surface profile data. Then the resulting data is a summation of a series of sine and cosine waves. The complex forms of the sine and cosine terms at each frequency are combined using a complex conjugate to provide the amplitude of the waveform at each scale for further calculations. Each frequency is considered a scale or layer of asperities which are stacked iteratively upon each other.

In its full form, the multiscale model of rough surface contact requires an iterative numerical algorithm to solve it, which can be difficult to implement for practicing engineers. Therefore the model can be simplified by making a few assumptions as was shown in [58]. In that work, it was shown that the real contact pressure (P_r) predicted by the multiscale model is approximated by the following equations from [58] for the elastic and elastic-plastic cases, respectively (a short derivation is provided in Appendix A):

$$(P_r)_{\text{elastic}} = \sqrt{2}\pi E' B_{\max} \tag{5a}$$

$$(P_r)_{\text{elastic/plastic}} = \sqrt{2}\pi E' B_{\max} \times \left[11 \Big/ \left(\frac{12\pi E'}{\sqrt{2} S_y e^{\frac{2}{3}\nu}} B_{\max} + 7\right)\right]^{3/5}. \tag{5b}$$

Subsequently, the contact force can be simply divided by the real contact pressure (P_r) to obtain the real area of contact (A_r) for elastic and elastic-plastic contact, respectively

$$(A_r)_{\text{elastic}} = \frac{F}{(P_r)_{\text{elastic}}} \tag{6a}$$

$$(A_r)_{\text{elastic/plastic}} = \frac{F}{(P_r)_{\text{elastic/plastic}}} \tag{6b}$$

where $B_{\max}$ is the maximum ratio of the amplitude to the wavelength acquired from the Fourier series of the surface. Equations (5a) and (5b) are derived from the pressures required to obtain complete contact between sinusoidal surfaces [24]. The current model decomposes the surface into a series of stacked sine waves and finds that the real contact pressure is only slightly smaller than the pressure required to flatten sine waves defined by $B_{\max}$. One question may then arise as to when to use the elastic or elastic-plastic solution. A critical value of the amplitude to wavelength ratio (B_c) is analytically derived in [24] using the von Mises yield criterion as

$$B_c = \frac{\sqrt{2}}{3\pi}\frac{S_y}{E'}e^{\frac{2}{3}\nu}. \tag{7}$$

Therefore when $B > B_c$, the contact is elastic-plastic and (6a) should be used; otherwise, (6b) should be used.

Using (5)–(7), the normalized contact pressure (P_r/S_y) can be mapped for different material property ratios (S_y/E') and amplitude to wavelength ratios (B), as shown in Fig. 2. The transition from elastic to elastic-plastic contact is shown by a red line. Above the red line, the model predicts elastic-plastic contact, and below it predicts only elastic contact. A dashed red box is shown to indicate the region that most engineering surfaces fall into, but there are still many other cases that fall outside this region.

Researchers in the field of nano and microscale mechanics of materials have found that the material properties of some materials change significantly with scale. Particularly, researchers such as Fleck and Hutchinson have found that the flow stress or yield strength S_y of a material can increase dramatically with smaller length scales [42]. These effects are due to the scale-dependent material features such as grains. Experimental methods such as nanoindentation tests and small-scale wire tests originally showed these effects and confirmed their existence.

One phenomenological theory that describes this effect is known as "strain gradient plasticity." Many subsequent works have studied strain gradient plasticity and derived models for it [22], [43]–[46], [59]–[61]. Hutchinson describes the implication of these effects and stresses how important it can be for these effects to be considered in modeling mechanics at the microscale [46]. The surface asperities of rough surfaces vary in size and shape and have been shown to span the size range of strain gradient plasticity effects [4], [23], [47], [48], [56], [62].

The plastic deformation that occurs at the tips of asperities in contact varies widely from nanoscale to macroscale strain. Due of this, scale effects that cause the yield strength of a material to effectively change with size should be considered. Again, these effects result from material features such as grain boundaries, which typically occur at a representative length scale but greatly affect plastic deformation. Nix and Gao [63] have formulated a model that describes the strain gradient effect on the change in material hardness with scale. This model was derived to account for these effects during nanoindentation tests. The strain-gradient-dependent hardness

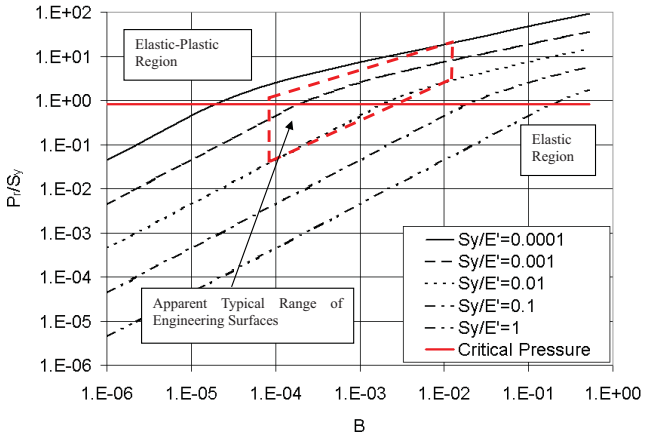

Fig. 2. Predictions of (6) and (7) as a function of B (or $B_{\max}$) and S_y/E'.

for Berkovich-type indenters is given by Nix and Gao as

$$H = H_o\sqrt{1+\frac{h^*}{h_p}} \tag{8}$$

where H_o is the macroscopic hardness, H is the corrected scale dependent hardness, and h_p is the depth of plastic deformation caused by the indentation. h^* is a material-dependent length scale which will change for different materials with different microstructures [63], [64]. In this paper, experimental results for the TCR of copper are considered and therefore a value of $h^* = 0.464\ \mu$m given for cold-worked polycrystalline copper by Nix and Gao [63] is used.

However, fundamentally the hardness is changing because the strain gradient effect changes the value of the yield strength S_y. S_y is a parameter in (5)–(7), and strain gradient plasticity should also be accounted for there. Similar to (8), the strain-gradient-dependent yield strength can be represented by

$$S_y = (S_y)_o\sqrt{1+\frac{h^*}{h_p}} \tag{9}$$

where $(S_y)_o$ is the yield strength without strain gradient effects (i.e., the bulk yield strength).

Now, a method for predicting the plastic indentation depth h_p at the asperity scale is required. For elastic-plastic sinusoidal contact, Krithivasan and Jackson [25] showed that the contact may "revert" back to elastic contact when complete contact occurs, because the stress state becomes hydrostatic. This was also shown by Manners [54] using fully plastic slip line theory. The simplified multiscale rough surface contact theory given by (6) predicts that many of the asperity contacts will flatten completely. In order to make an approximate prediction of the plastic indentation depth, we assume here that the asperity scale with the highest amplitude to wavelength ratio is flattened. If we assume that the contact reverts to an elastic state, then an effective deformed amplitude can be found by setting the average pressure required to obtain complete contact between elastic sinusoidal surfaces [65]

$$p^* = \sqrt{2}\pi E'\Delta f \tag{10}$$

equal to the average pressure required to obtain complete contact between elastic-plastic sinusoidal surfaces

$$\frac{P_P^*}{P^*} = \left(\frac{11}{4\cdot(\Delta/\Delta c)+7}\right)^{3/5} \tag{11}$$

where

$$\Delta c = \frac{\sqrt{2}\cdot S_y \exp\left(\frac{2\upsilon}{3}\right)}{3\pi E' f} \tag{12}$$

which results in

$$p^* = \sqrt{2}\pi E' \Delta_{\text{def}} f = p_p^* = \sqrt{2}\pi E' \Delta f \left(\frac{11}{4\cdot(\Delta/\Delta c)+7}\right)^{3/5}. \tag{13}$$

Then, simplifying and noting that the difference between the deformed amplitude and the original amplitude is the plastic indentation depth h_p, we get

$$h_p = \Delta - \Delta_{\text{def}} = \Delta\left[1-\left(\frac{11}{4\cdot(\Delta/\Delta c)+7}\right)^{3/5}\right]. \tag{14}$$

Here, h_p is found from (14), which depends on the critical interference Δ_c among the other parameters. Since Δ_c (12) is dependent on S_y, (9) and (14) are coupled. Physically, this simply shows that the contact of rough surfaces is dependent on the scale of local asperity surface deformations, which suggests that it cannot be easily described by macroscale global properties. In this paper, (9) and (14) are solved simultaneously using an iterative scheme. However, it is highly desirable to provide a closed-form prediction. In an attempt to find an approximate solution, (12) is substituted in (14) and normalized

$$\frac{h_p}{\Delta} = \left[1-\left(\frac{11}{12\pi E' B \Big/ \sqrt{2}S_y \exp(2\upsilon/3)+7}\right)^{3/5}\right]. \tag{15}$$

Then normalizing (9) by $E'/\exp(2\upsilon/3)$, and substituting in $B_{\max}$, $\Delta_{\max}$ and (15) results in

$$\frac{S_y \exp(2\upsilon/3)}{E'} = \frac{\left(S_y\right)_o \exp(2\upsilon/3)}{E'}\sqrt{1+\frac{h^*}{\Delta_{\max}}\frac{\Delta_{\max}}{h_p}} = \frac{\left(S_y\right)_o \exp(2\upsilon/3)}{E'} \times \sqrt{1+\frac{h^*}{\Delta_{\max}}\left[1-\left(\frac{11}{\frac{12\pi E' B_{\max}}{\sqrt{2}S_y \exp(2\upsilon/3)}+7}\right)^{3/5}\right]^{-1}}. \tag{16}$$

Equation (16), which can be used to solve for $S_y \exp(2\upsilon/3)/E'$, is then a function of the nondimensional parameters $h^*/\Delta_{\max}$, $\left(S_y\right)_o \exp(2\upsilon/3)/E'$, and $B_{\max}$. $\left(S_y\right)_o \exp(2\upsilon/3)/E'$ is the ratio of macroscale material properties, which for metals is usually around 1/1000, but for small-scale objects that possess a perfect lattice, the ratio for the scale-dependent properties, $S_y \exp(2\upsilon/3)/E'$, could reach 1/10. $B_{\max}$ is a geometric description of the rough surface, and more specifically describes the "roughness" by relating the asperity amplitude to wavelength. Finally, $h^*/\Delta_{\max}$ is a parameter that quantifies the scale of the contact and is similar to the Knudsen number. As $h^*/\Delta_{\max}$ approaches unity, the scale effects will become more influential. Note that, as $S_y \exp(2\upsilon/3)/E'$ increases, eventually it will cause B_c to become equal to $B_{\max}$, which will cause the contact to revert to an elastic one. This limiting value can be found by rearranging (12) as

$$\frac{3\pi B_{\max}}{\sqrt{2}} = \left(\frac{S_y \exp(2\upsilon/3)}{E'}\right)_c. \tag{17}$$

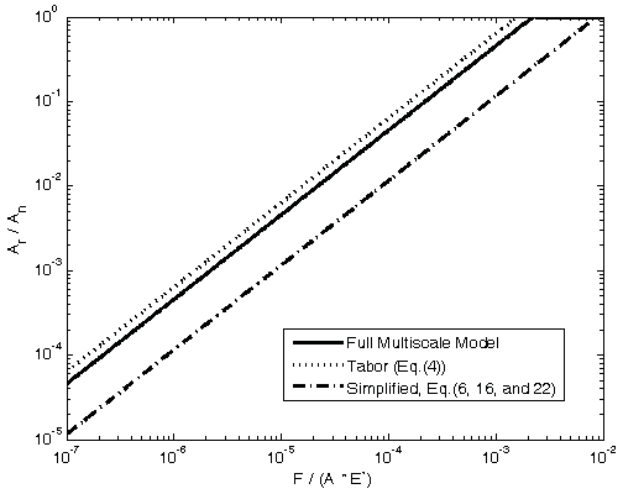

Fig. 3. Predicted contact area of several theoretical elastic-plastic contact models.

To illustrate the influence these scale-dependent properties have on the contact of rough surfaces, the predicted real area of contact is plotted as a function of the load for the new simplified model while including scale-dependent yield strength (6) and (16), the full iterative multiscale elastic plastic contact model [57], and the classic hardness based prediction (4). This is shown in Fig. 3. The two latter models do not include scale-dependent yield strength, and the hardness-based prediction is actually independent of the surface roughness. Note that both multiscale models predict a smaller area of contact because they consider how the surface geometry can increase the contact pressure past the classic definition of hardness. Finally, the simplified model predicts a much smaller contact area because it also includes the effect of scale-dependent material properties, which may be very important in modeling the contact of small-scale asperities.

B. Simplified Multiscale Contact Resistance Model

The multiscale rough surface contact model's predictions of the real area of contact are then used to predict contact resistance. Holm [66] gives a simple formula to calculate the electrical and thermal resistance due to asperity contact

$$R_{\text{asp}} = \frac{\left(k_1^{-1}+k_2^{-1}\right)}{4a_c} = \frac{1}{4a_c k} \tag{18}$$

where R_{asp} refers to the resistance value, a_c is the radius of contact, k_1, k_2 are the thermal conductivity of the respective surfaces, and k is the conductivity if the two surfaces are

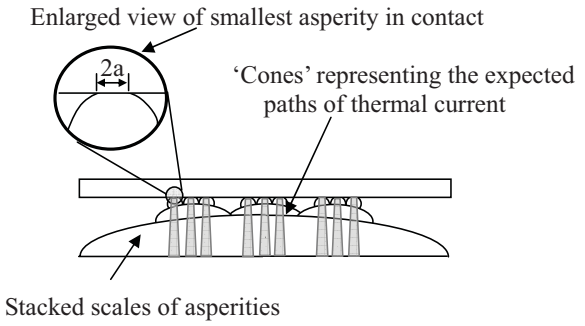

Fig. 4. Schematic of a simplified multiscale perspective of contact resistance.

assumed to be the same material. The TCR predicted by (18) is good only for a single asperity. In the case of both multiscale and statistical techniques, additional equations are required to calculate resistance for the entire surface.

In a previous work on multiscale TCR, the entire iterative procedure is outlined in detail [34], but here we remove the need for iterations and simplify the model. The conduction or resistance part of the simplified model is similar to that presented for electrical contact resistance in Jackson *et al*. [67]. It is assumed that each scale of asperities can be modeled as an evenly spaced cluster of contacts with the same contact radius that are effectively routed in parallel. The simplified version of the alleviation factor offered by Cooper *et al*. [68] is also used between scales. The scales are then considered to be routed in series and so the contact resistance from each scale is summed over all the possible iteration levels to find the total resistance for the entire surface in contact resulting in (this equation was previously presented in [34] and [57])

$$R_{\text{total}} = \sum_{i=1}^{i_{\max}} R_i / (\eta_i A_i). \tag{19}$$

Equation (19) must be calculated iteratively and is used to calculate the resistance for the full multiscale model that will be compared with the simplified closed-form model that is derived next. It is important to note that this technique calculates the resistance for each frequency level and then sums over all frequency levels to calculate the total. In order to simplify (19), the multiple scales of stacked asperities are now considered using a single cone-shaped asperity concept (see Fig. 4). Consider the geometry of a single asperity in contact located on top of the stacks of larger scale asperities. If it is assumed that each of the smallest scale contacts is isolated, then the multispot contact resistance can be approximated by

$$R_c = \frac{1}{4 a_c k n}. \tag{20}$$

Then a method is required to find a_c and n. To find a_c, one can consider the predicted real contact area, and from that divide by the number of contact spots (asperities) and assume that they are circular, which gives

$$a_c = \left(\frac{A_r}{\pi n}\right)^{1/2}. \tag{21}$$

Finally, the number n of asperities in contact, as predicted by the multiscale model, must be calculated. As each scale of asperities is included in the multiscale model, the real area of contact is reduced. This also results in the increase in real contact pressure. The pressure will increase until the maximum value of B in the surfaces' Fourier series is reached ($B_{\max}$). The wavelength at which this occurs is $\lambda_{\max}$. Since there are two asperity peaks in contact for one square wavelength area of the sinusoidal surface

$$n = 2\frac{A_r}{\lambda_{\max}^2}. \tag{22}$$

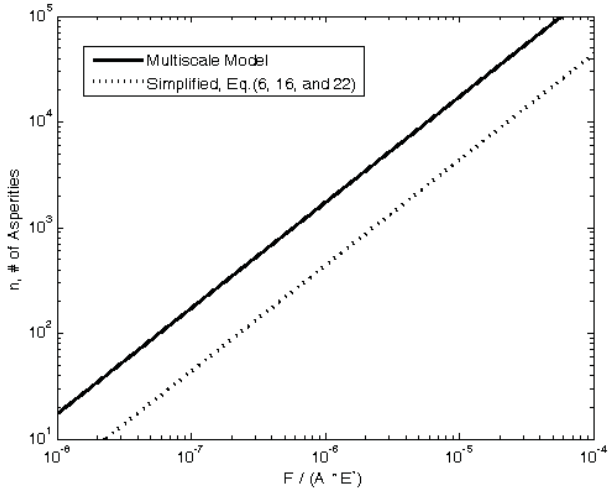

Fig. 5. Number of asperities in contact as a function of load as predicted by the models.

The predictions of the simplified multiscale model, given by substituting (6) and (16) into (22), are compared with those of the full multiscale rough surface contact model (see Fig. 5). Note that the scale-dependent material yield strength effect is included in the simplified model and not in the multiscale model, and that is responsible for most of the quantitative disagreement between the models. The inclusion of scale-dependent yield strength effectively strengthens the asperities in contact and thus reduces the area of contact and the number of asperities in contact. Qualitatively, they both predict that the number of asperities in contact will increase with load.

Next, to find the average contact radius, (22) is substituted into (21), resulting in

$$a_c = \frac{\lambda_{\max}}{\sqrt{2\pi}}. \tag{23}$$

Then substituting (22) and (23) into (20) results in the simple relationship

$$R_c = \frac{\sqrt{2\pi}}{2k}\left(\frac{\lambda_{\max}}{2A_r}\right). \tag{24}$$

The real area of contact A_r in (24) can be predicted by (6) for elastic-plastic deformation, resulting in

$$R_c = \frac{\pi^{3/2} E' \Delta_{\max}}{2kF}\left[\frac{11}{12\pi E' B_{\max} / \left(\sqrt{2} S_y e^{\frac{2}{3}\nu}\right) + 7}\right]^{3/5}. \tag{25}$$

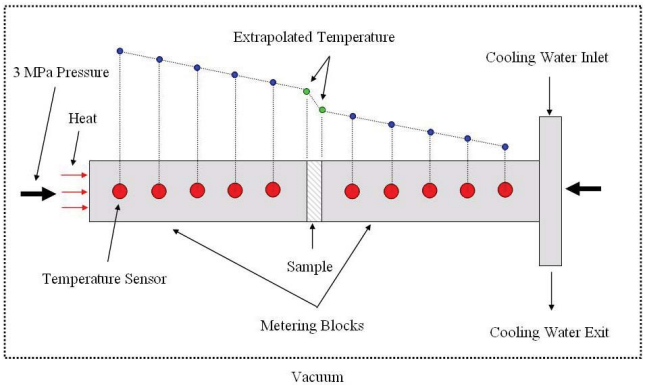

Fig. 6. Theory of operation of apparatus used to measure thermal resistance of thin components.

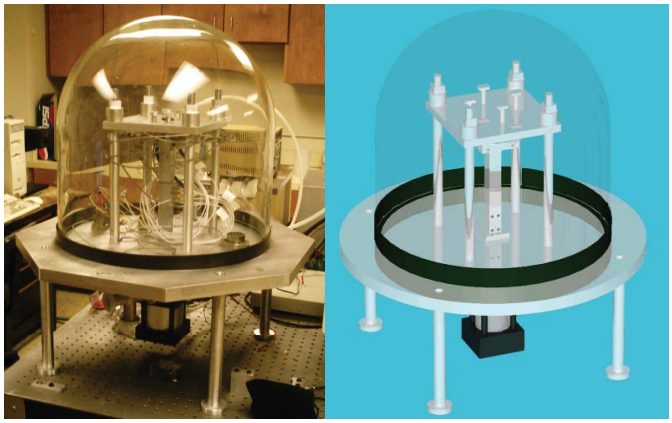

Fig. 7. Solid model and photograph of the apparatus.

Note that, to account for the scale dependence of the yield strength, the result of (16) is substituted into (25) for $S_y \exp(2\upsilon/3)/E'$. In addition, (25) only accounts for the contact resistance of one surface in contact with a flat rigid surface. Therefore, for two equivalent surfaces in contact, the resistance would simply be multiplied by a factor of 2 (this assumes that the surfaces are symmetric about the plane of the contact area). The assumption of symmetry should be fairly accurate since heat is flowing through fairly isolated contact spots. On one side the heat will constrict, and on the other it will expand. The shape of the heat flow should therefore be symmetric although it is flowing only in one direction. Similarly, for purely elastic contact, (5) can be substituted into (24) instead, resulting in

$$R_c = \frac{\pi^{3/2} E' \Delta_{\max}}{2kF}. \tag{26}$$

Note that (16) and (25) are all that is needed to calculate the contact resistance because (6) is included in (25). Likewise, (5) is included in (26). Note, again, that to consider two rough surfaces in contact, (26) must be multiplied by 2.

III. Experimental Methodology

The experiments used for comparison with the simplified multiscale model of contact resistance were actually conducted independently and several years before the derivation of the multiscale contact model technique [69]. The goal of the experimental work was to measure the bulk conductive properties of materials. As will be discussed in more detail, to measure the thermal resistance across the bulk material, the contact resistance had to be removed. The measurement of contact resistance was therefore a necessary by-product of the previous work that employed the ASTM standard D5470-95 experimental arrangement.

ASTM standard D5470-95 offers an alternative nonintrusive approach to measure thermal resistance of thin components used in electronic packaging. The apparatus consists of two long metering blocks featuring equispaced holes for temperature sensor insertion. The first metering block (hot metering block) is heated by means of several electric heaters attached to one of its ends. The opposing end of the other metering block (cold metering block) is attached to a serpentine tube through which the cooling fluid flows. The sample to be examined, which has a cross-sectional area identical to that of the metering blocks, is placed in between the free ends of the two metering blocks, and an axial pressure of up to 3 MPa is applied. The whole assembly is placed in vacuum to minimize heat loss to the environment. Placing the samples in vacuum could also limit the amount of oxide on the surfaces, which could affect the contact resistance.

A. Test Apparatus Description

Heaters attached to the base of the hot metering block generate heat that flows through the hot metering block, the sample, the cold metering block, and, ultimately, the cooling serpentine. The heat flow generates a temperature drop across the metering blocks and the sample. The temperature drop across the metering blocks is sensed using the temperature sensors embedded inside the metering blocks. By knowing the thermal conductivity of the metering block material and the temperature drop across any of the metering blocks, the heat Q flowing through the stack may be calculated. The temperature drop across the thin sample is then calculated by extrapolating temperature measurements in the cold and hot metering blocks to the sample's lower and upper surfaces. The thermal conductivity of the sample can then be calculated as

$$k_s = \frac{Q}{A_s} \frac{L_s}{\Delta T_s}. \tag{27}$$

A schematic of the theory of operation for the apparatus is shown in Fig. 6.

The apparatus was constructed from aluminum alloy 2024-T3. It included a pneumatic actuator that was capable of applying up to 2358 N of axial force and attached to the bottom of a base plate. The metering blocks and cooling serpentine were allowed to slide freely on four cylindrical guides mounted on the upper surface of a base plate. The sliding movement was restricted to a maximum of 25 mm, which defined the maximum sample thickness. A compressive force from the actuator was transmitted to the metering blocks through a rubber diaphragm which also acted as vacuum seal. The value of the axial force was measured using a load cell

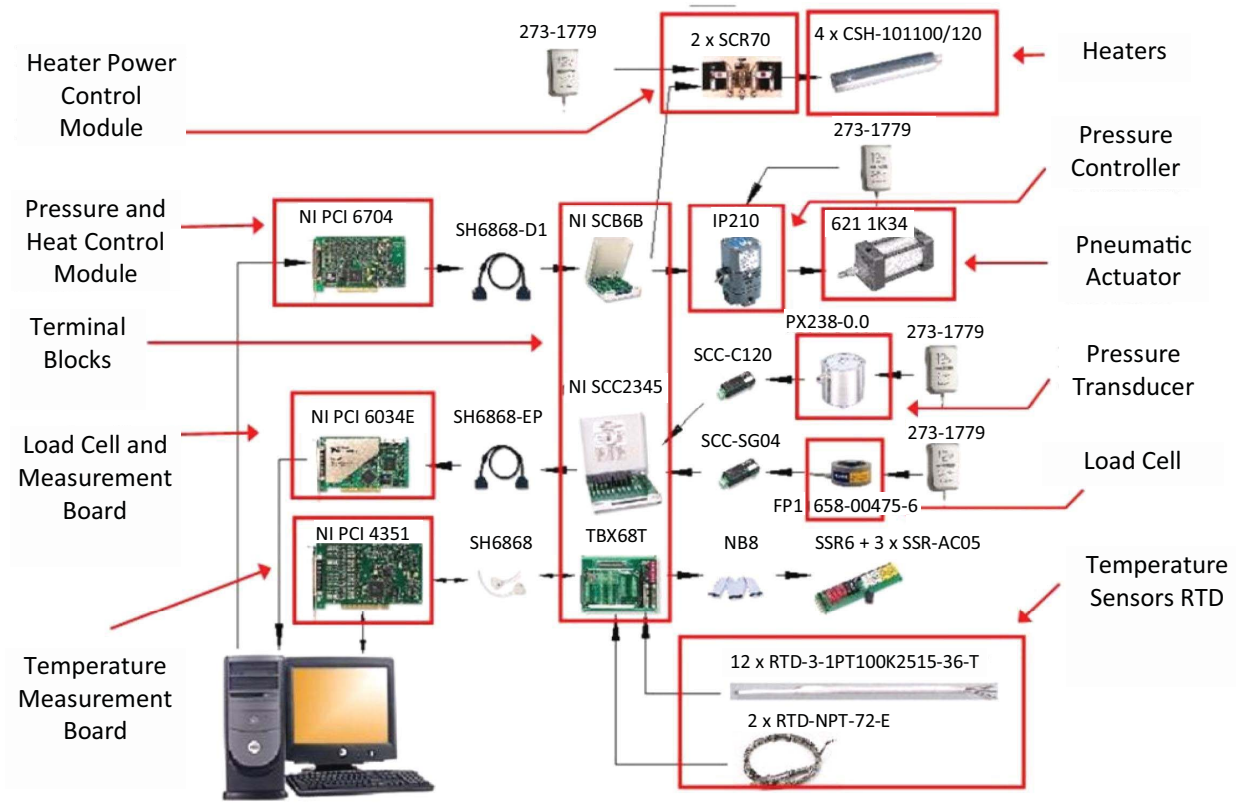

Fig. 8. Data acquisition and control diagram.

TABLE I
MEASUREMENTS USED TO CALCULATE CONTACT RESISTANCE (5-mm-THICK SAMPLE)

Force [N]	Q [W] hot block	Q [W] cold block	Q [W] average	ΔT [K] sample	Mean sample temperature [°C]
890	27.02	27.32	27.17	4	50.02
1134	27.11	27.4	27.26	3.73	49.97
1357	27.1	27.52	27.31	3.64	50.04
1579	27.29	27.5	27.4	3.53	50
1802	27.44	27.61	27.53	3.45	50.05
2015	27.5	27.58	27.54	3.38	50.01
2282	27.38	27.74	27.56	3.29	50.06
2464	27.49	27.71	27.6	3.25	50.06
2691	27.46	27.78	27.62	3.19	50.05
2918	27.45	27.79	27.62	3.12	50.03
3114	27.72	27.9	27.81	3.05	50.05

TABLE II
MEASUREMENTS USED TO CALCULATE CONTACT RESISTANCE (10-mm-THICK SAMPLE)

Force [N]	Q [W] hot block	Q [W] cold block	Q [W] average	ΔT [K] sample	Mean sample temperature [°C]
890	26.88	27.21	27.05	4.18	50.03
1223	27.23	27.29	27.26	3.98	50.01
1348	27.07	27.41	27.24	3.92	50.03
1601	27.15	27.49	27.32	3.8	50.05
1788	27.34	27.48	27.41	3.75	50.05
2024	27.25	27.61	27.43	3.65	50.09
2251	27.32	27.61	27.47	3.6	50.06
2460	27.23	27.58	27.41	3.56	50.02
2673	27.23	27.55	27.39	3.53	50.04
2918	27.26	27.62	27.44	3.49	50.07
3132	27.13	27.66	27.4	3.44	50.07

sandwiched between the serpentine and a stationary stopper. Water and electrical feed-through connectors were attached to the base plate to allow routing of cooling water, power, and measurement signals to the vacuum environment.

A solid model of the apparatus and an image of the apparatus after assembly are shown in Fig. 7. Near the bottom of the hot metering block, four through holes arranged in a 2×2 matrix housed cylindrical cartridge heaters capable of a maximum output of 400 W. The heaters were wired such that upper two heaters heated the metering blocks while the lower two heaters acted as guard heaters. Two extra resistance temperature detectors (RTDs) were placed in between the upper and lower rows of heaters to balance heat flow. The data acquisition system also collected force readings from the load cell and the vacuum pressure from a vacuum gauge fitted to the vacuum line. Fig. 8 shows the details of the components used in data acquisition and control.

B. Evaluation of Sample Contact Resistance

In the previous experimental study [69], it was important to evaluate contact resistance since it is usually of considerable value and cannot be overlooked. To evaluate the contact resistance between the sample and metering blocks, two

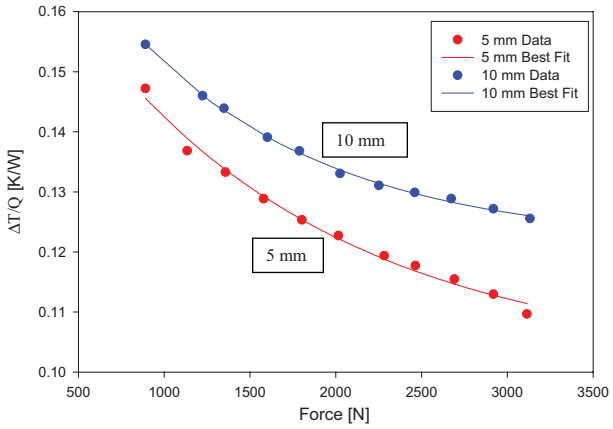

Fig. 9. Thermal resistance measurements of 5-mm and 10-mm copper samples.

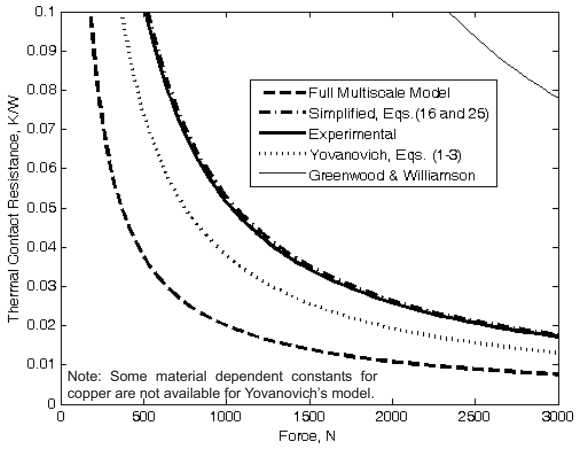

Fig. 10. Comparison between several TCR models and experimental measurements of copper contacts.

25-mm × 25-mm copper samples of 5-mm and 10-mm thickness were tested. Copper was selected as the sample material because it would be a good indicator of the accuracy of the measurement device because of its low thermal resistance. Since both samples were of the same material and varied only in thickness, thermal resistance of the 10-mm sample should be double that of the 5-mm sample if TCR was negligible. Therefore, the relation between the thermal resistances of the two samples can be written as

$$R_{\text{th\_10 mm}} = 2R_{\text{th\_5 mm}} \tag{28}$$

where

$$R_{\text{th\_10 mm}} + R_C = \frac{\Delta T_{10}}{Q_{10}} \tag{29}$$

$$R_{\text{th\_5 mm}} + R_C = \frac{\Delta T_5}{Q_5}. \tag{30}$$

Multiplying (30) by 2 gives

$$2R_{\text{th\_5 mm}} + 2R_C = 2\frac{\Delta T_5}{Q_5}. \tag{31}$$

Substituting for $2R_{\text{th\_5 mm}}$ with $R_{\text{th\_10 mm}}$, (31) becomes

$$R_{\text{th\_10 mm}} + 2R_C = 2\frac{\Delta T_5}{Q_5}. \tag{32}$$

Subtracting (29) from (32) yields the contact resistance as

$$R_C = 2\frac{\Delta T_5}{Q_5} - \frac{\Delta T_{10}}{Q_{10}}. \tag{33}$$

By repeating measurements for the 10-mm and 5-mm samples under different axial loads, it was be possible to generate calibration curves that were used to account for contact resistance for different samples under different axial loads. The tests were performed for both samples under a vacuum of less than 3 mTorr. The applied axial force varied from 890 to 3114 N with an approximate step size of 222 N. At every step, the heat flow through the sample and temperature drop across the sample were calculated. The average sample temperature through the test was kept at 50 ± 0.1 °C.

Measurements used to calculate TCR are listed in Tables I and II. Due to differences in the calculated heat flow values between the cold and hot metering blocks, the average of the two metering blocks was used. However, at any given step, the mismatch between the two metering blocks did not exceed 2%. Thermal resistance versus axial force data were fitted with an exponential equation of the form

$$R_{\text{th}} = ae^{\text{bF}} + c. \tag{34}$$

The correlation coefficients for the 5-mm sample were

$$a = 0.080158 \text{ K/W}, \quad b = -6.750824 \times 10^{-4} 1/\text{N},$$
$$c = 0.101625 \text{ K/W}.$$

The correlation coefficients for the 10-mm sample were

$$a = 0.072374 \text{ K/W}, \quad b = -8.731265 \times 10^{-4} 1/\text{N},$$
$$c = 0.121281 \text{ K/W}.$$

The measured $\Delta T/Q$ values and the corresponding best fit curves are shown in Fig. 9. Substituting the best fit equations into (33) results in

$$R_c = 2\left(0.080158e^{-6.750824E-4F} + 0.101625\right) - \left(0.072374e^{-8.731265E-4F} + 0.121281\right) \text{ K/W} \tag{35}$$

which is rearranged to

$$R_c = 0.160316e^{-6.750824E-4F} - 0.072374e^{-8.731265E-4F} + 0.081969 \text{ K/W}. \tag{36}$$

A plot of contact resistance versus axial force is shown in Fig. 10 alongside the theoretical prediction derived earlier in this paper as well as in other existing models. These results are discussed in greater detail in the next section.

IV. Experimental and Theoretical Comparison

The TCR was calculated using the new simplified multiscale model given by (6), (16), and (22). Surface profiles of the original copper test samples [69] were recorded using a Veeco Dektak 150 stylus profilometer (see Fig. 11). The surface profiles were nearly the same, no matter what the orientation

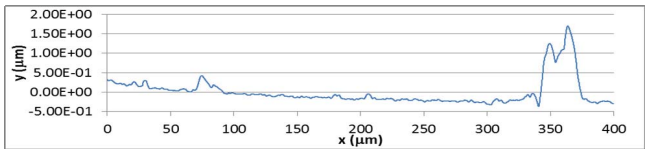

Fig. 11. Surface profile of the copper sample.

TABLE III
MATERIAL AND SURFACE PROPERTIES OF COPPER SAMPLES

$E = 119$ GPa [70]	$(S_y)_o = 70$ MPa [71]
$\upsilon = 0.326$ [70]	$K = 401$ W/m · K [72]
$h^* = 0.464$ μm [63]	$H = 196$ MPa
$B_{\max} = 1.628 \times 10^{-3}$	$\lambda = 18.18$ μm
$\sigma = 0.352$ μm	$c_o = -0.26$
$m = 0.0283$	

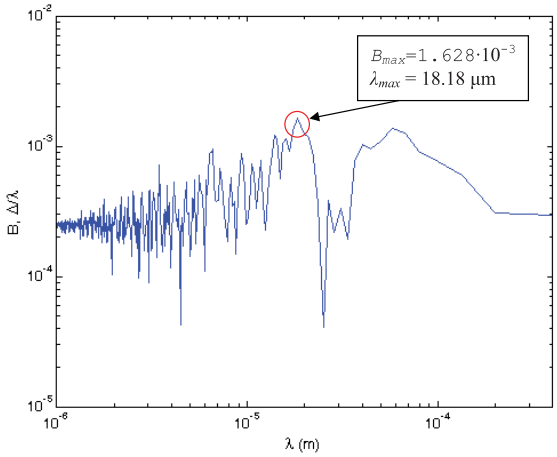

Fig. 12. Values of the amplitude to wavelength ratio for different wavelength scales using an FFT of the surface data.

or location on the surface, so only one representative scan was used for the calculations presented in this paper. The statistical parameters needed for the GW model [5] and Yovonovich model [4], such as RMS roughness σ and the effective absolute surface slope m, were calculated using the methods outlined in [73]. The GW model [5] is also briefly summarized in Appendix B. For the multiscale models, an FFT of the surface data was also taken and the complex conjugate of each of the terms at each wavelength λ was used to calculate the amplitude Δ. Then the ratio of the amplitude to the wavelength (B) at each wavelength was calculated and plotted as shown in Fig. 12. For use in the new simplified model (25) and (26), the highest value of $B(B_{\max})$ was found to be 1.628×10^{-3} at a wavelength ($\lambda_{\max}$) of 18.18 μm.

In this paper, experimental results for the TCR of copper will be considered and therefore a value of $h^* = 0.464$ μm given for cold-worked polycrystalline copper by Nix and Gao [63] is used in (16). The other material properties used in this paper, including the bulk yield strength, are listed in Table III. Note that for Yovanovich's model [4] given by (1)–(3), the bulk hardness H was set to the conventional value of 2.8 S_y.

Using (16) and (25), the contact resistance was calculated for the rough surface contacting a perfectly flat surface, and then doubled to considered the equivalent case of two rough surfaces in contact. This assumes that the copper surfaces in contact are practically of identical roughness, which was also found from profilometry measurements. Next, the model [(16) and (25)] was compared with the predictions of the empirical model given by Yovanovich [4] [(1)–(3)] along with the perfectly elastic GW model [5] given by (A10), as shown in Fig. 10. Note that the many more recent elastic-plastic extensions of the GW model [56], [74]–[76] are not considered here because there are no closed-form solutions to the most advanced models that include finite element-based asperity models [21], [77] that can be easily implemented without numerical methods.

The TCR predicted by the GW [5] statistical perfectly elastic model is greater than the other two models probably because it does not account for plastic deformation, the effects of scaling, or the interaction between adjacent asperities. Notice that the full iterative elastic-plastic multiscale model [57] also does not compare well with the experimental values, but this is probably due to it not including the effect of the scale-dependent yield strength. However, Yovanovich's model [4] is in relatively close agreement with the experimental results (an average error of 32.3%), and the new multiscale model appears to be in almost exact agreement. Note that this agreement is obtained without the use of any fitting parameters, which is extremely surprising since the new simplified mutliscale model is entirely theoretically derived. Both of these models do consider the effect of scale-dependent yield strength, which is probably why they compare the best. However, the model by Yovanovich is empirically derived using materials different from copper and therefore may need to be slightly adjusted to match the copper measurements.

Another reason for the differences between the three models is how the contact resistance is calculated from the asperity distribution and sizes. The statistical perfectly elastic model [5] considers asperities of a constant radius but with different contact radii a, depending on their individual height and amount of loading. However, the full iterative and simplified multiscale models calculate the number of asperities by considering the average size and wavelength of the asperities in contact and determine the distribution this way. Of course, Yovanovich's empirical model [4] does not need to predict the size or distribution of asperity contacts at all.

The differences between the results of the models and the experimental measurements could also be due to thermal expansion at the asperity level. There is not yet a practical model to predict the temperature distribution of each asperity and then the associated thermal expansion without performing a computationally costly finite element analysis of every single asperity (because each is of a different size and under different loads). However, an analysis using Hertz contact and Holm's equation also shows that the effect of thermal expansion appears to be negligible, at least for the current case and likely for most cases (see Appendix C for details).

All of the models appear to predict the same overall trend (see Fig. 10), but they vary in the degree of quantitative

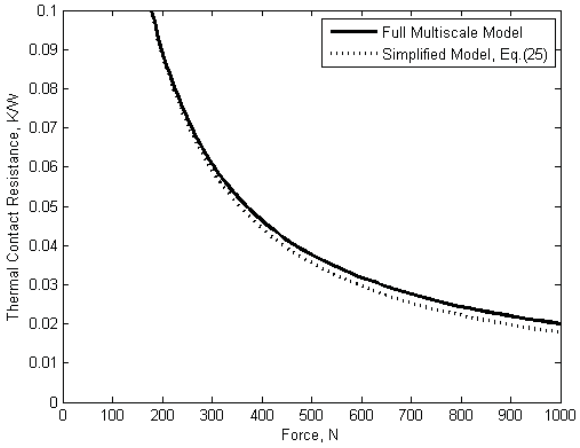

Fig. 13. Comparison of the TCR predicted by the full multiscale model and the simplified multiscale model without scale-dependent properties.

agreement. Since only one experimental result for copper is presented here, additional measurements are needed to further verify the accuracy of these models for different conditions. One should also use care in employing these models because of the simplifications they make in modeling the surface geometry and contact mechanics. The differences seen between the full multiscale model and simplified model, as shown in Figs. 3, 5, and 10, are mostly due to the inclusion of the scale-dependent yield strength. To illustrate this, the TCR predicted by the simplified model (25) and the full multiscale model, without including scale-dependent properties in either, is shown in Fig. 13. Although there are differences due to the assumptions made in order to simplify the model to a single equation, these differences are relatively small compared to the effect of the scale-dependent yield strength, as shown in Fig. 12.

V. Conclusion

In this paper, we presented a new simplified method of calculating elastic-plastic TCR based upon a multiscale model of rough surfaces built on stacked sinusoids [see (25), (26), and other supporting equations). Results from this new technique have also been compared with the pre-existing elastic statistical methods and empirical methods presented by Yovanovich [4]. The models all show the same trends, but the simplified multiscale model derived in this paper [(16), (25), and (26)] appears to show the best agreement with the experimental measurements of a prior independently conducted study. Yovanovich's model also appears to make reasonable predictions and, as with the new multiscale model, also includes the effect of scale-dependent yield strength. The difference between Yovanovich's model results and those of the experiment may be because was the former was based on fitting to the experimental results of other materials. The statistical elastic model by GW does predict the correct trend but does not produce good quantitative agreement, perhaps because it was purely elastic and does not consider the effects of various scales of roughness.

Appendix A
Abbreviated Derivation of Simplified Multiscale Contact Model

Equation (5) is mathematically derived using the theory of elastic superposition, but for a more detailed explanation and discussion one should refer to [58]. First, consider a series of sinusoidal surfaces which together describe the multiscale topography of a surface. For simplicity, the 2-D Fourier series will be used here, but other series using different scaling techniques may also be used

$$z(x) = \sum_{n=1}^{\infty} a_n \cos\left(2\pi n \frac{x}{\lambda} + \phi_n\right). \tag{A1}$$

Now consider that, to obtain complete contact, all the scales need to be flattened out. First, consider the largest scale of features ($n = 1$) on the surface, the pressure distribution needed to obtain complete contact is

$$p_1(x) = p_1^* \left[1 + \cos\left(2\pi \frac{x}{\lambda} + \phi_1\right)\right]. \tag{A2}$$

Now consider the next smaller scale of features, and the pressure required to obtain complete contact is

$$p_2(x) = p_2^* \left[1 + \cos\left(4\pi \frac{x}{\lambda} + \phi_2\right)\right]. \tag{A3}$$

Then, by using the theory of elastic superposition, the pressure profile required to obtain complete contact between a flat surface and a surface containing the two largest scale terms of the Fourier series is given by

$$p_{1-2}(x) = p_1^* + p_1^* \cos\left(2\pi \frac{x}{\lambda} + \phi_1\right) + \max\left[p_2^* - p_1^*, 0\right] + p_2^* \cos\left(4\pi \frac{x}{\lambda} + \phi_2\right). \tag{A4}$$

Note that the first and third terms on the right-hand side of (A4) represent the average pressures at each scale. As each smaller scale is included, only the average pressure needs to be increased if the average pressure of the smaller scale (p_2^*) is larger than the average pressure of the first scale (p_1^*). The second and fourth terms represent the oscillation of the pressure over the surface. Equation (A4) can then be expanded for the case considering all of the scales of the surface given by (A1). The resulting pressure profile for complete contact of the surface is then

$$p(x) = p_1^* + p_1^* \cos\left(2\pi \frac{x}{\lambda} + \phi_1\right) + \sum_{n=2}^{\infty} \left\{\max\left[p_n^* - \max\left[p_{n-1}^*, \ldots, p_1^*\right], 0\right] + p_n^* \cos\left(2\pi n \frac{x}{\lambda} + \phi_n\right)\right\}. \tag{A5}$$

By combining the average pressure terms (denoted by superscript *), this can then be simplified further to

$$p(x) = \max\left[p_1^*, \ldots, p_\infty^*\right] + \sum_{n=1}^{\infty} p_n^* \cos\left(2\pi n \frac{x}{\lambda} + \phi_n\right). \tag{A6}$$

For calculating the real area of contact between surfaces, one needs only the average contact pressure. Therefore, by

calculating the average pressure of the surface from (A6), the following is obtained:

$$p_{\text{ave}} = \max\left[p_1^*, \ldots, p_\infty^*\right]. \tag{A7}$$

which is identical to (5) if one considers that the average pressure to obtain complete contact between a multiscale surface and a flat surface is also the same as the pressure needed to obtain contact between the rough surfaces so long as the scale of the considered roughness is less than the scale of the contact area. For instance, if the maximum p^* occurs at a small scale, then the contact area will be significantly larger for most loads. For elastic-plastic contact, it might not be applicable because elastic superposition cannot be employed. One encouraging point is that [25], [24], [54] have found that, for elastic-plastic sinusoidal surfaces in complete contact, the deformation appears to effectively revert to elastic deformation. Then the use of superposition might again be valid and applicable to the elastic-plastic case as given by (5b). Again, additional details about this model can be found in [58].

APPENDIX B

PERFECTLY ELASTIC STATISTICAL MODEL

The GW model [5] of rough surface contact assumes that the asperities follow a height distribution Φ, and all have a radius of curvature at their tips R. The area and load are calculated using an integral of Φ and a function relating the asperity height z to the surface separation d. All asperities in the range $z > d$ will be in contact with the rigid flat. The compression distance $z - d$ is the interference of the rigid flat with the asperity peaks and is known as ω for the remainder of this paper. The resulting integrals for TCR and load are

$$\frac{1}{R_c} = \frac{2A_n\eta\sqrt{\beta}}{\rho}\int_{\cdot d}^{\cdot\infty}\sqrt{z-d}\cdot\Phi(z)\cdot dz \tag{B1}$$

$$F = A_n\eta\int_{\cdot d}^{\cdot\infty}\bar{F}(\omega)\cdot\Phi(z)\cdot dz. \tag{B2}$$

For the perfectly elastic case, the values of $\bar{F}$ are acquired from the Hertz solutions, given as

$$\bar{F} = \frac{4}{3}E'\sqrt{\beta}\,(\omega)^{3/2}. \tag{B3}$$

As this is a statistical method, it hinges upon obtaining statistical parameters that describe the surface. To this end, the spectral moments of the surfaces are calculated by

$$M_2 = \frac{1}{N}\sum_{n=1}^{N}\left(\frac{dz}{dx}\right)_n^2 \tag{B4}$$

$$M_4 = \frac{1}{N}\sum_{n=1}^{N}\left(\frac{d^2z}{dx^2}\right)_n^2 \tag{B5}$$

where N is the total number of data points on the surface and z is the distance from the mean height of the surface to the asperity peak. The radius of curvature β and the areal asperity density η are then calculated by the method of [78] using spectral moments (26), (27) about the surface

$$\eta = \left(\frac{M_4}{M_2}\right)\cdot\left(\frac{1}{6\pi\sqrt{3}}\right) \tag{B6}$$

$$\beta = 0.375\cdot\left(\frac{\pi}{M_4}\right)^{0.5}. \tag{B7}$$

Instead of a Gaussian distribution for the asperity heights, GW suggest using an exponential distribution so that the equations can be analytically solved. The resulting solutions found in GW are given as

$$\frac{1}{R_c} = \frac{\sqrt{\pi}\,A_n\eta\sqrt{\sigma\beta}}{\rho}e^{-d} \tag{B8}$$

$$F = E'A_n\sqrt{\pi\sigma/\beta}\,(\eta\beta\sigma)\,e^{-d}. \tag{B9}$$

Then substituting (B9) into (B8) results in the following closed-form prediction of TCR:

$$R_c = \frac{\rho\sigma E'}{F}. \tag{B10}$$

APPENDIX C

SIMPLE EVALUATION OF THE EFFECT OF THERMAL EXPANSION AT THE ASPERITY SCALE

This section verifies the neglect of thermal expansion in this paper, although it may still be important in some cases. First, simplifying a single asperity as a 1-D heat transfer problem, the TCR for a single asperity is calculated from Holm's equation and related to the heat flow and temperature change by

$$R_{\text{asp}} = \frac{1}{4a_ck} = \frac{\Delta T}{Q_{\text{asp}}}. \tag{C1}$$

If the asperities are modeled as spheres and the effect of the surface and the asperities base is neglected, then the thermal expansion would effectively increase the radius of the sphere by

$$\beta_t = \beta(1+\alpha\Delta T). \tag{C2}$$

Then from Hertz contact, the contact radius can be predicted by

$$a_c = \left(\frac{3\bar{F}R\beta_t}{4E'}\right)^{1/3}. \tag{C3}$$

However, since the multiscale analysis used in this paper assumes that the asperities are sinusoidal in shape, the radius of curvature at the tips of the smallest asperities reducing the area of contact can be predicted by

$$\beta = \frac{\lambda_{\max}}{4\pi^2 B_{\max}}. \tag{C4}$$

Finally, solving for the temperature and substituting (C2) and (C3) into (C1), the following is obtained:

$$\Delta T = \frac{Q_{\text{asp}}}{4k}\left(\frac{3\bar{F}R\lambda_{\max}(1+\alpha\Delta T)}{16\pi^2E'B_{\max}}\right)^{-1/3}. \tag{C5}$$

Equation (C5) then provides an approximate prediction of the temperature rise across a single asperity. Note that, if the

heat flow is evenly divided by the number of asperities in contact, then the heat flow across each asperity is approximated by $Q_{\text{asp}} = Q/n$, where n is given by (21). The number of asperities n will also affect the force on each asperity and here it is assumed that the force on each asperity is approximately $\bar{F} = F/n$.

The cases mostly likely to be effected by thermal expansion are at low loads and pressures because contact patches will be small, causing the most TCR. At a nominal pressure of 1 MPa, which is lower than that in the current experiments, the number of asperities in contact is approximately 10 000 according to the multiscale model (see Fig. 5). Assuming the material properties and surface properties in Table III (along with $\alpha = 16.6\ \mu\text{m/m}^\circ\text{K}$), and that $Q = 27$ W, (C5) is solved and the temperature rise across an asperity is predicted to be approximately 0.4 K. Then the asperity radius changes by less than 0.01% and the change in contact resistance due to thermal expansion is practically immeasurable according to the current analysis. Other reasonable combinations of loads and numbers of asperities have also been considered, all resulting in a negligible change in contact resistance.

REFERENCES

[1] M. A. Lambert and L. S. Fletcher, "Review of models for thermal contact conductance of metals," *J. Thermophys. Heat Transfer*, vol. 11, no. 2, pp. 129–140, 1997.

[2] C. V. Madhusudana and L. S. Fletcher, "Contact heat transfer - The last decade," *AIAA J.*, vol. 24, pp. 510–523, Mar. 1986.

[3] C. V. Madhusudana, L. S. Fletcher, and G. P. Peterson, "Thermal conductance of cylindrical joints - A critical review," *J. Thermophys. Heat Transfer*, vol. 4, pp. 204–211, Apr. 1990.

[4] M. M. Yovanovich, "Four decades of research on thermal contact, gap, and joint resistance in microelectronics," *IEEE Trans. Compon. Packag. Technol.*, vol. 28, no. 2, pp. 182–206, Jun. 2005.

[5] J. A. Greenwood and J. B. P. Williamson, "Contact of nominally flat surfaces," *Proc. Royal Soc. London A*, vol. 295, no. 1442, pp. 300–319, 1966.

[6] L. Kogut and R. L. Jackson, "A comparison of contact modeling utilizing statistical and fractal approaches," *ASME J. Tribol.*, vol. 128, no. 1, pp. 213–217, 2005.

[7] A. Majumdar and C. L. Tien, "Fractal characterization and simulation of rough surface," *Wear*, vol. 136, no. 2, pp. 313–327, 1990.

[8] Y. Z. Li, C. V. Madhusudana, and E. Leonardi, "Experimental investigation of thermal contact conductance: Variations of surface microhardness and roughness," *Int. J. Thermophys.*, vol. 19, no. 6, pp. 1691–1704, 1998.

[9] M. Borri-Brunetto, A. Carpinteri, and B. Chiaia, "Scaling phenomena due to fractal contact in concrete and rock fractures," *Int. J. Fracture*, vol. 95, nos. 1–4, pp. 221–238, 1999.

[10] M. Borri-Brunetto, B. Chiaia, and M. Ciavarella, "Incipient sliding of rough surfaces in contact: A multiscale numerical analysis," *Comp. Methods Appl. Mech. Eng.*, vol. 190, nos. 46–47, pp. 6053–6073, 2001.

[11] S. Hyun, L. Pel, J. F. Molinari, and M. O. Robbins, "Finite-element analysis of contact between elastic self-affine surfaces," *Phys. Rev. E*, vol. 70, no. 2, pp. 026117-1–026117-12, 2004.

[12] K. Komvopoulos and N. Ye, "Three-demensional contact analysis of elastic-plastic layered media with fractal surface topographies," *ASME J. Tribol.*, vol. 123, no. 3, pp. 632–640, 2001.

[13] A. Majumdar and B. Bhushan, "Fractal model of elastic-plastic contact between rough surfaces," *ASME J. Tribol.*, vol. 113, no. 1, pp. 1–11, 1991.

[14] T. L. Warren and D. Krajcinovic, "Fractal models of elastic-perfectly plastic contact of rough surfaces based on the cantor set," *Int. J. Solids Struct.*, vol. 32, no. 19, pp. 2907–2922, 1995.

[15] K. Willner, "Elasto-plastic normal contact of 3-D fractal surfaces using halfspace theory," *ASME J. Tribol.*, vol. 126, no. 1, pp. 28–33, 2004.

[16] W. Yan and K. Komvopoulos, "Contact analysis of elastic-plastic fractal surface," *J. Appl. Phys.*, vol. 84, no. 7, pp. 3617–3624, 1998.

[17] M. M. Chaudhri, I. M. Hutchings, and P. L. Makin, "Plastic compression of spheres," *Philosoph. Mag.*, vol. 49, no. 4, pp. 493–503, 1984.

[18] S. D. Mesarovic and N. A. Fleck, "Frictionless indentation of dissimilar elastic-plastic spheres," *Int. J. Solids Struct.*, vol. 37, nos. 46–47, pp. 7071–7091, 2000.

[19] L. Kogut and K. Komvopoulos, "Analysis of spherical indentation cycle of elastic-perfectly plastic solids," *J. Mater. Res.*, vol. 19, no. 12, pp. 3641–3653, 2004.

[20] R. L. Jackson, "The effect of scale dependant hardness on elasto-plastic asperity contact between rough surfaces," *STLE Tribol. Trans.*, vol. 49, no. 2, pp. 135–150, 2006.

[21] R. L. Jackson and I. Green, "A finite element study of elasto-plastic hemispherical contact," *ASME J. Tribol.*, vol. 127, no. 3, pp. 343–354, 2005.

[22] Y. Wei and J. W. Hutchinson, "Hardness trends in micron scale indentation," *J. Mech. Phys. Solids*, vol. 51, nos. 11–12, pp. 2037–2056, 2003.

[23] M. M. Yovanovich and A. Hegazy, "An accurate universal contact conductance correlation for conforming rough surfaces with different micro-hardness profiles," in *Proc. AIAA 18th Thermophys. Conf.*, Montreal, QC, Canada, 1983, pp. 1–7.

[24] R. L. Jackson, V. Krithivasan, and W. E. Wilson, "The pressure to cause complete contact between elastic plastic sinusoidal surfaces," *IMechE J. Eng. Tribol. J*, vol. 222, no. 7, pp. 857–864, 2008.

[25] V. Krithivasan and R. L. Jackson, "An analysis of 3-D elasto-plastic sinusoidal contact," *Tribol. Lett.*, vol. 27, no. 1, pp. 31–43, 2007.

[26] S. S. Wadwalkar, R. L. Jackson, and L. Kogut, "A study of the elastic-plastic deformation of heavily deformed spherical contacts," *IMechE J, J. Eng. Tribol.*, vol. 224, no. 10, pp. 1091–1102, 2010.

[27] R. L. Jackson and J. L. Streator, "A multiscale model for contact between rough surfaces," *Wear*, vol. 261, nos. 11–12, pp. 1337–1347, 2006.

[28] L. Almeida, R. Ramadoss, R. Jackson, K. Ishikawa, and Q. Yu, "Laterally actuated multi-contact MEMS relay fabricated using metalMUMPS process: Experimental characterization and multiscale contact modeling," *J. Micro/Nanolith. MEMS/MOEMS*, vol. 6, no. 2, p. 023009, 2007.

[29] C. K. Bora, E. E. Flater, M. D. Street, J. M. Redmond, M. J. Starr, R. W. Carpick, and M. E. Plesha, "Multiscale roughness and modeling of MEMS interfaces," *Tribol. Lett.*, vol. 19, no. 1, pp. 37–48, 2005.

[30] M. Ciavarella, G. Demelio, J. R. Barber, and Y. H. Jang, "Linear elastic contact of the weierstrass profile," *Proc. Royal Soc. London A*, vol. 456, no. 1994, pp. 387–405, 2000.

[31] M. Ciavarella, G. Murolo, G. Demelio, and J. R. Barber, "Elastic contact stiffness and contact resistance for the weierstrass profile," *J. Mech. Phys. Solids*, vol. 52, no. 6, pp. 1247–1265, 2004.

[32] M. K. Thompson, "A multi-scale iterative approach for finite element modeling of thermal contact resistance," Ph.D. dissertation, Dept. Mech. Eng., Massachusetts Inst. Technol., Cambridge, 2007.

[33] M. K. Thompson and J. M. Thompson, "Considerations for the incorporation of measured surfaces in finite element models," *Scanning*, vol. 32, no. 4, pp. 183–198, 2010.

[34] R. L. Jackson, S. H. Bhavnani, and T. P. Ferguson, "A multi-scale model of thermal contact resistance between rough surfaces," *ASME J. Heat Transfer*, vol. 130, no. 8, pp. 081301-1–081301-8, 2008.

[35] S. Saha and L. Shi, "Molecular dynamics simulation of thermal transport at nanometer size point contacts on a planar silicon substrate," in *Proc. ASME Conf.*, San Francisco, CA, 2005, pp. 389–396.

[36] L. Weber, E. Gmelin, and H. J. Queisser, "Thermal resistance of silicon point contacts," *Phys. Rev. B*, vol. 40, no. 2, pp. 1244–1249, 1989.

[37] L. Weber, M. Lehr, and E. Gmelin, "Investigation of the transport properties of gold point contacts," *Phys. B, Condens. Matter*, vol. 217, nos. 3–4, pp. 181–192, 1996.

[38] W. A. Little, "The transport of heat between dissimilar solids at low temperatures," *Canadian J. Phys.*, vol. 37, no. 3, pp. 334–349, 1959.

[39] G. Chen, "Nonlocal and nonequilibrium heat conduction in the vicinity of nanoparticles," *J. Heat Transfer*, vol. 118, no. 3, pp. 539–545, 1996.

[40] R. Prasher, "Predicting the thermal resistance of nanosized constrictions," *Nano Lett.*, vol. 5, no. 11, pp. 2155–2159, 2005.

[41] G. Chen, "Nanoscale heat transfer and nanostructured thermoelectrics," in *Proc. Intersoc. Conf. Thermomech. Phenomena Electron. Syst.*, Las Vegas, NV, 2004, p. 8.

[42] N. A. Fleck and J. W. Hutchinson, "A phenomenological theory for strain gradient effects in plasticity," *J. Mech. Phys. Solids*, vol. 41, no. 12, pp. 1825–1857, 1993.

[43] N. A. Fleck, G. M. Muller, M. F. Ashby, and J. W. Hutchinson, "Strain gradient plasticity: Theory and experiment," *Acta Metall. Mater.*, vol. 42, no. 2, pp. 475–487, 1994.

[44] H. Gao, Y. Huang, W. D. Nix, and J. W. Hutchinson, "Mechanism-based strain gradient plasticity—I. Theory," *J. Mech. Phys. Solids*, vol. 47, no. 6, pp. 1239–1263, 1999.
[45] H. Gao, Y. Huang, W. D. Nix, and J. W. J. Hutchinson, "Mechanism-based strain gradient plasticity—II. Analysis," *J. Mech. Phys. Solids*, vol. 48, no. 1, pp. 99–128, 2000.
[46] J. W. Hutchinson, "Plasticity at the micron scale," *Int. J. Solids Struct.*, vol. 37, nos. 1–2, pp. 225–238, 2000.
[47] L. Almeida, R. Ramadoss, R. Jackson, K. Ishikawa, and Q. Yu, "Laterally actuated multicontact MEMS relay fabricated using metalMUMPS process: Experimental characterization and multiscale contact modeling," *J. Micro/Nanolith. MEMS MOEMS*, vol. 6, no. 2, p. 023009, 2007.
[48] S. Song and M. M. Yovanovich, "Relative contact pressure: Dependence on surface roughness and vickers microhardness," *J. Thermophys.*, vol. 2, no. 1, pp. 43–47, 1988.
[49] A. Hegazy, "Thermal joint conductance of conforming rough surfaces: Effect of surface micro-hardness variation," Ph.D. thesis, Univ. Waterloo, Waterloo, ON, Canada, 1985.
[50] M. K. Thompson, "Finite element modeling of multi-scale thermal contact resistance (MNHT2008–52385)," in *Proc. ASME 1st Int. Conf. Micro/Nanoscale Heat Transfer*, Tainan, Taiwan, 2008, pp. 509–517.
[51] B. N. J. Persson, "Elastoplastic contact between randomly rough surfaces," *Phys. Rev. Lett.*, vol. 87, no. 11, pp. 116101-1–116101-4, 2001.
[52] D. Tabor, *The Hardness of Materials*. Gloucestershire, U.K.: Clarendon, 1951.
[53] J. Pullen and J. B. P. Williamson, "On the plastic contact of rough surfaces," *Proc. Royal Soc. London A*, vol. 327, no. 1569, pp. 159–173, 1972.
[54] W. Manners, "Plastic deformation of a sinusoidal surface," *Wear*, vol. 264, nos. 1–2, pp. 60–68, 2008.
[55] J. F. Archard, "Elastic deformation and the laws of friction," *Proc. Royal Soc. London A*, vol. 243, no. 1233, pp. 190–205, 1957.
[56] R. L. Jackson, "The effect of scale dependant hardness on elasto-plastic asperity contact between rough surfaces," *STLE Tribol. Trans.*, vol. 49, no. 2, pp. 135–150, 2006.
[57] W. E. Wilson, S. V. Angadi, and R. L. Jackson, "Surface separation and contact resistance considering sinusoidal elastic-plastic multi-scale rough surface contact," *Wear*, vol. 268, nos. 1–2, pp. 190–201, Jan. 2010.
[58] R. L. Jackson, "An analytical solution to an archard-type fractal rough surface contact model," *Tribol. Trans.*, vol. 53, no. 4, pp. 543–553, 2010.
[59] J. Y. Shu and N. A. Fleck, "The prediction of a size effect in micro-indentation," *Int. J. Solids Struct.*, vol. 35, no. 13, pp. 1363–1383, 1998.
[60] M. Zhao, W. S. Slaughter, M. Li, and S. X. Mao, "Material-length-scale-controlled nanoindentation size effects due to strain-gradient plasticity," *Acta Mater.*, vol. 51, no. 15, pp. 4461–4469, 2003.
[61] R. Rodriquez and I. Gutierrez, "Correlation between nanoindentation and tensile properties: Influence of indentation size effect," *Mater. Sci. Eng., A*, vol. A361, nos. 1–2, pp. 377–384, 2003.
[62] B. Bhushan and M. Nosonovsky, "Scale effects in friction using strain gradient plasticity and dislocation-assisted sliding (microslip)," *Acta Mater.*, vol. 51, no. 14, pp. 4331–4345, Aug. 2003.
[63] W. D. Nix and H. Gao, "Indentation size effects in crystalline materials: A law for strain gradient plasticity," *J. Mech. Phys. Solids*, vol. 46, no. 3, pp. 411–425, 1998.
[64] J. G. Swadener, E. P. George, and G. M. Pharr, "The correlation of the indentation size effect measured with indenters of various shapes," *J. Mech. Phys. Solids*, vol. 50, no. 4, pp. 681–694, 2002.
[65] K. L. Johnson, J. A. Greenwood, and J. G. Higginson, "The contact of elastic regular wavy surfaces," *Int. J. Mech. Sci.*, vol. 27, no. 6, pp. 383–396, 1985.
[66] R. Holm, *Electric Contacts*. New York: Springer-Verlag, 1967.
[67] R. L. Jackson, R. D. Malucci, S. Angadi, and J. R. Polchow, "A simplified model of multiscale electrical contact resistance and comparison to existing closed form models," in *Proc. 55th IEEE Holm Conf. Electr. Contacts*, Vancouver, BC, Canada, Sep. 2009, pp. 1–15.
[68] M. G. Cooper, B. B. Mikic, and M. M. Yovanovich, "Thermal contact conductance," *Int. J. Heat Mass Transfer*, vol. 12, no. 3, pp. 279–300, 1969.
[69] Y. A. Elkady, "Thermal performance of ball grid arrays and thin interface materials," Ph.D. dissertation, Dept. Mech. Eng., Auburn Univ., Auburn, AL, 2005.
[70] J. E. Shigley and C. R. Mischke, *Mechanical Engineering Design*, 5th ed. New York: McGraw-Hill, 1989.
[71] R. C. Hibbeler, *Mechanics of Materials*, 8th ed. New York: Pearson, 2011.
[72] F. P. Incropera and D. P. DeWitt, *Fundamentals of Heat and Mass Transfer*, 4th ed. New York: Wiley, 1996.
[73] J. I. McCool, "Relating profile instrument measurements to the functional performance of rough surfaces," *ASME J. Tribol.*, vol. 109, no. 2, pp. 264–270, 1987.
[74] W. R. Chang, I. Etsion, and D. B. Bogy, "An elastic-plastic model for the contact of rough surfaces," *ASME J. Tribol.*, vol. 109, no. 2, pp. 257–263, 1987.
[75] R. L. Jackson and I. Green, "A statistical model of elasto-plastic asperity contact between rough surfaces," *Tribol. Int.*, vol. 39, no. 9, pp. 906–914, 2006.
[76] L. Kogut and I. Etsion, "A finite element based elastic-plastic model for the contact of rough surfaces," *Tribol. Trans.*, vol. 46, no. 3, pp. 383–390, 2003.
[77] L. Kogut and I. Etsion, "Elastic-plastic contact analysis of a sphere and a rigid flat," *ASME J. Appl. Mech.*, vol. 69, no. 5, pp. 657–662, 2002.
[78] J. I. McCool, "Comparison of models for the contact of rough surfaces," *Wear*, vol. 107, no. 1, pp. 37–60, 1986.

Robert L. Jackson received the B.S., M.S., and Ph.D. degrees in mechanical engineering from the Georgia Institute of Technology, Atlanta, in 1998, 2000, and 2004, respectively.

He is currently an Associate Professor of mechanical engineering with Auburn University, Auburn, AL. His current research interests include multiscale tribology, contact mechanics, lubrication, electrical and thermal contact resistance, surface texturing, and fundamentals of friction and wear.

Hamed Ghaednia received the B.S. and M.S. degrees in mechanical engineering and the B.S. degree in chemical engineering from the Amirkabir University of Technology (Tehran Polytechnic), Tehran, Iran, in 2006, 2010, and 2010, respectively. He is currently pursuing the Ph.D. degree in tribology (mechanical engineering) with Auburn University, Auburn, AL.

He was with the Parsian Robotic Group, Tehran Polytechnic, Tehran, and a Graduate Assistant with the Vibration and Noise Control Laboratory, Tehran Polytechnic. He has published papers in the fields of vibration control, magneto-rheological bearings, and contact mechanics. His current research interests include nanoparticle lubricants, nanotribology, and contact mechanics.

Yasser A. Elkady author photograph and biography not available at the time of publication.

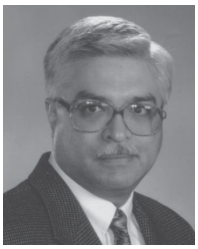

Sushil H. Bhavnani is a Professor of mechanical engineering with Auburn University, Auburn, AL. He has published over 110 refereed journal and conference publications. His current research interests include liquid cooling of electronics.

He is a fellow of the American Society of Mechanical Engineers. He was the co-recipient of the Clock Award in 2008 for sustained contributions to the area of electronics packaging and the ASME Curriculum Innovation Award in 1999 for a live internet-delivered course on thermal management of electronics. He has been serving on the American Society of Mechanical Engineers (ASME)-HTD K-16 Committee on heat transfer in electronic equipment since 1989. In 1998, he served as the General Chairman of the Intersociety Conference on Thermal and Thermomechanical Phenomena in Electronic Systems. He currently serves on the Executive Committee of this conference and as its Awards Co-Chair. In 2003, he served as the Awards Chair of InterPack, the International Electronic Packaging Technical Conference and Exhibition. He has been an Associate Editor of the IEEE TRANSACTIONS ON COMPONENTS, PACKAGING AND MANUFACTURING TECHNOLOGY since 2001.

Roy W. Knight author photograph and biography not available at the time of publication.